AFRL-RZ-WP-TP-2012-0143

ENHANCEMENT AND ANGULAR DEPENDENCE OF TRANSPORT CRITICAL CURRENT DENSITY IN PULSED LASER DEPOSITED $YBa_2Cu_3O_{7-x}$+$BaSnO_3$ FILMS IN APPLIED MAGNETIC FIELDS (POSTPRINT)

C.V. Varanasi, J. Burke, and L. Brunke

University of Dayton Research Institute

H. Wang

Texas A&M University

M. Sumption

The Ohio State University

P.N. Barnes

Mechanical Energy Conversion Branch
Energy/Power/Thermal Division

FEBRUARY 2012

AIR FORCE RESEARCH LABORATORY
PROPULSION DIRECTORATE
WRIGHT-PATTERSON AIR FORCE BASE, OH 45433-7251
AIR FORCE MATERIEL COMMAND
UNITED STATES AIR FORCE

REPORT DOCUMENTATION PAGE

Form Approved
OMB No. 0704-0188

1. REPORT DATE *(DD-MM-YY)*	2. REPORT TYPE	3. DATES COVERED *(From - To)*
February 2012	Journal Article Postprint	04 April 2005 – 04 April 2007

4. TITLE AND SUBTITLE

ENHANCEMENT AND ANGULAR DEPENDENCE OF TRANSPORT CRITICAL CURRENT DENSITY IN PULSED LASER DEPOSITED $YBa_2Cu_3O_{7-x}$+$BaSnO_3$ FILMS IN APPLIED MAGNETIC FIELDS (POSTPRINT)

5a. CONTRACT NUMBER
In-house

5b. GRANT NUMBER

5c. PROGRAM ELEMENT NUMBER
62203F

6. AUTHOR(S)

C.V. Varanasi, J. Burke, and L. Brunke (University of Dayton Research Institute)
H. Wang (Texas A&M University)
M. Sumption (The Ohio State University)
P.N. Barnes (AFRL/RZPG)

5d. PROJECT NUMBER
3145

5e. TASK NUMBER
32

5f. WORK UNIT NUMBER
314532ZE

7. PERFORMING ORGANIZATION NAME(S) AND ADDRESS(ES)

University of Dayton Research Institute
Dayton, OH 45469

Texas A&M University
College Station, TX 77843

The Ohio State University
Columbus, OH 43210

Mechanical Energy Conversion Branch (AFRL/RZPG)
Energy/Power/Thermal Division
Air Force Research Laboratory, Propulsion Directorate
Wright-Patterson Air Force Base, OH 45433-7251
Air Force Materiel Command, United States Air Force

8. PERFORMING ORGANIZATION REPORT NUMBER
AFRL-RZ-WP-TP-2012-0143

9. SPONSORING/MONITORING AGENCY NAME(S) AND ADDRESS(ES)

Air Force Research Laboratory
Propulsion Directorate
Wright-Patterson Air Force Base, OH 45433-7251
Air Force Materiel Command
United States Air Force

10. SPONSORING/MONITORING AGENCY ACRONYM(S)
AFRL/RZPG

11. SPONSORING/MONITORING AGENCY REPORT NUMBER(S)
AFRL-RZ-WP-TP-2012-0143

12. DISTRIBUTION/AVAILABILITY STATEMENT

Approved for public release; distribution unlimited.

13. SUPPLEMENTARY NOTES

Journal article published *Journal of Applied Physics*, Vol. 102, 2007.

 PA Case Number: AFRL/WS-07-0145; Clearance Date: 04 Apr 2007. Work on this effort was completed in 2007. This paper has color content.

14. ABSTRACT

$YBa_2Cu_3O_{7-x}$ (YBCO) films with nanoparticles of $BaSnO_3$ (BSO) were processed using pulsed laser ablation of a special target made with dual phase sectors of YBCO and BSO. Transport critical current density (J_{ct}) of these YBCO+BSO films in applied magnetic fields and angular dependence of J_{ct} on the applied field orientation was measured. It was observed that in the YBCO+BSO films, the J_{ct} ($H \| c$ orientation) increased considerably as compared to regular YBCO films and was 1.3 times higher than J_{ct} in H $\|ab$ orientation. Cross-sectional transmission electron microscopy images on YBCO+BSO films showed the presence of high density (3.5×10^{11} cm^{-2}) of nanoparticles (~10 nm size) and nanocolumns that extended throughout the thickness of the films with high density of dislocations and stacking faults (1000 μm^{-2}). The observed results of enhancements in J_{ct} in $H \| c$ and J_{ct} in H $\|ab$ orientations were discussed in the light of the observed microstructural details.

15. SUBJECT TERMS

dual phase sectors, nanoparticles, thickness, microstructural, high density, applied field orientation, transports, laser ablation

16. SECURITY CLASSIFICATION OF:			17. LIMITATION OF ABSTRACT:	18. NUMBER OF PAGES	19a. NAME OF RESPONSIBLE PERSON (Monitor)
a. REPORT	b. ABSTRACT	c. THIS PAGE			Timothy J. Haugan
Unclassified	Unclassified	Unclassified	SAR	12	19b. TELEPHONE NUMBER *(Include Area Code)* N/A

Enhancement and angular dependence of transport critical current density in pulsed laser deposited $YBa_2Cu_3O_{7-x}+BaSnO_3$ films in applied magnetic fields

C. V. Varanasi,[a] J. Burke, and L. Brunke
University of Dayton Research Institute, Dayton, Ohio 45469, USA

H. Wang
Texas A&M University, College Station, Texas 77843, USA

M. Sumption
The Ohio State University, Columbus, Ohio 43210, USA

P. N. Barnes
Air Force Research Laboratory, Wright-Patterson AFB, Ohio 45433, USA

(Received 18 May 2007; accepted 25 July 2007; published online 25 September 2007)

$YBa_2Cu_3O_{7-x}$ (YBCO) films with nanoparticles of $BaSnO_3$ (BSO) were processed using pulsed laser ablation of a special target made with dual phase sectors of YBCO and BSO. Transport critical current density (J_{ct}) of these YBCO+BSO films in applied magnetic fields and angular dependence of J_{ct} on the applied field orientation was measured. It was observed that in the YBCO+BSO films, the J_{ct} ($H\|c$ orientation) increased considerably as compared to regular YBCO films and was 1.3 times higher than J_{ct} in $H\|ab$ orientation. Cross-sectional transmission electron microscopy images on YBCO+BSO films showed the presence of high density (3.5×10^{11} cm^{-2}) of nanoparticles ($\sim$10 nm size) and nanocolumns that extended throughout the thickness of the films with high density of dislocations and stacking faults (1000 μm^{-2}). The observed results of enhancements in J_{ct} in $H\|c$ and J_{ct} in $H\|ab$ orientations were discussed in the light of the observed microstructural details. © *2007 American Institute of Physics*. [DOI: 10.1063/1.2783783]

I. INTRODUCTION

Improvements in the critical current density (J_c) in applied magnetic fields are of great importance for $YBa_2Cu_3O_{7-x}$ (YBCO) coated conductors to be used in applications such as high temperature superconducting (HTS) generators and motors.[1] Flux pinning enhancement in YBCO films is one of the principal means to improve J_c in applied magnetic fields. The introduction of nanoparticles into YBCO films has been demonstrated as a viable method to introduce the required flux pinning centers for the YBCO coated conductors.[2–5] In addition to acting as flux pinning centers by themselves, the nanoparticles can also create defects, such as strain fields surrounding the particles, stacking faults, and dislocations, that can potentially enhance the flux pinning. Since the coils in HTS rotating machinery experience various magnetic field vectors, it is important to obtain pinning enhancements in all possible orientations of the applied magnetic field.

In undoped YBCO films, the J_{ct} is higher in the $H\|ab$ orientation than the $H\|c$ orientation due to the intrinsic pinning offered by the layered structure of YBCO.[6] Ideally, the pinning should maximize the transport current in the coated conductors while minimizing the angular dependence of the conductor to avoid a preferred orientation. This makes coil fabrication for HTS machines much simpler by avoiding field dependent designs. The addition of flux pinning centers could change this anisotropic behavior of YBCO behavior by introducing c-axis correlated defects.[7] Since the addition of flux pinning centers could affect the angular dependence of J_{ct}, it is of interest to correlate the structure-property relationships in YBCO films processed with nanoparticles.

Several pinning materials including Y_2BaCuO_5, $BaZrO_3$, $BaIrO_3$, Nd_2O_3, YSZ, Y_2O_3, and $BaSnO_3$ (Refs. 2 and 8–13) have previously been investigated to improve the flux pinning properties of YBCO films. Depending upon the processing method, the composition, pinning material content, size, and distribution all determine the effectiveness of the nanoparticles for pinning enhancement. These differences in nanoparticle materials and processing methods result in YBCO films with pinning centers that can pin differently for particular magnetic field ranges. Hence, there is a need to identify a suitable material and processing method that will incorporate the nanoparticles in a manner that will obtain the desired effect.

Recently, YBCO+BSO (BSO=$BaSnO_3$) films were reported to have high J_c in applied magnetic fields showing more than an order of magnitude increase in J_c, determined by magnetization measurements in $H\|c$ orientation at high fields >2 T.[13] These films were deposited using a pulsed laser ablation method, where a special target made with dual phase sectors was used. Nonlayered nanoparticles of Y_2BaCuO_5 and BSO were introduced[4,13] using this method with considerable J_c improvements in YBCO. Melle *et al.*[11] also recently showed improvements in YBCO+YSZ (YSZ denotes yttria-stabilized zirconia) films processed by using

[a]Electronic mail: chakrapani.varanasi@wpafb.af.mil

0021-8979/2007/102(6)/063909/5/$23.00

an YBCO target with a YSZ sector. In the present paper, the critical transport current (J_{ct}) measurements in applied magnetic fields and angular dependence of YBCO+BSO films processed by dual phase sector method were investigated. Cross-sectional transmission electron microscopy (TEM) results are presented, and the observed J_{ct} results are discussed in the light of the observed microstructures.

II. EXPERIMENT

All the samples studied in the present work were processed by employing a pulsed laser ablation method using a dual sector pulsed laser deposition (PLD) target method as discussed in detail elsewhere.[13] Briefly, in this method, a thin sector (30° angle) cut from a disk of a sintered BSO target was attached to a top surface of an YBCO target. As the target was rotated, the BSO surface was ablated periodically, allowing the formation of BSO nanoparticles in the growing YBCO film. Due to the lattice mismatch between BSO and YBCO, nanoparticles were formed as opposed to continuous layers. All the depositions were done in a Neocera PLD chamber. A Lambda Physik KrF excimer laser (wavelength $\lambda = 248$ nm) was used to deposit films at an energy density of 2–4 J/cm^2. The films were grown at a 4 Hz repetition rate. The substrate temperature was maintained at 780 °C during the deposition, while the substrate to target distance was set at 6 cm. The target was rotated at a speed of 15–20 rpm during the deposition of YBCO+BSO nanocomposite film. Films with ~300 nm thickness were deposited on (100) $LaAlO_3$ single crystal substrates as well as on buffered biaxially textured Ni–W metallic substrates.

The pulsed laser ablation method discussed above with the dual phase sector target uses a single target to make the films in a scalable, continuous process. A particular advantage of this approach over a premixed target approach is that any possible chemical reactions between the pinning material and the YBCO in the target preparation stage are prevented as the second phase is physically separated from YBCO. The reaction time between the pinning material and YBCO coatings is reduced as the growth of the nanoparticles occurs simultaneously with the growth of YBCO film. Also, nanoparticles are introduced in a nonlayered fashion in contrast to an alternating target approach. The dual sector deposition approach provides a quick evaluation of different compositions by changing the second phase sector while maintaining the same YBCO target, thus avoiding differences that might be partially ascribed to differences in the batch of YBCO powder used.

The J_{ct} of the samples were measured by using a four probe transport current measurement method. Samples were prepared with 1–2 mm wide bridges using either laser ablation or chemical etch methods. The J_{ct} angular dependence was measured by rotating the sample through a range of −20° to 120° about the sample normal in an applied magnetic field of 1–5 T at 77 K. The J_{ct} data were collected every 2° near $H \| c$ and $H \| ab$ orientations and every 4° elsewhere. A voltage criterion of 1 μv/cm was used in the *I-V* curves obtained at various angles to determine the I_c and calculate J_c.

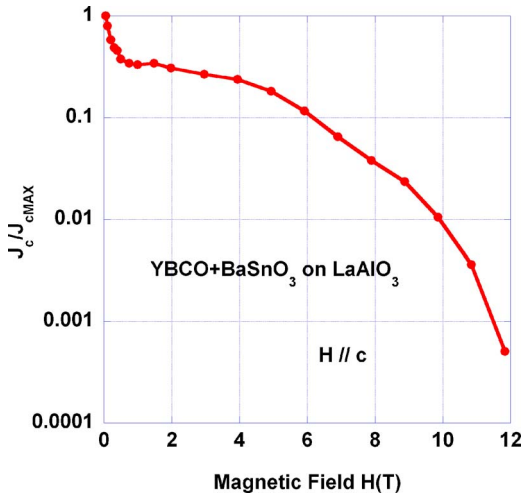

FIG. 1. Normalized plot of transport critical current density (J_{ct}) in applied magnetic field of an YBCO+BSO sample on $LaAlO_3$ substrate at 77 K.

The film microstructure was studied by using a SIRION high resolution scanning electron microscope (SEM). The cross-section TEM samples were prepared through a conventional TEM sample preparation technique involving gluing, grinding, polishing, and ion milling. The detailed microstructure of these samples was characterized by TEM and high resolution TEM using a JEOL-2010 analytical electron microscope with a point-to-point resolution of 0.21 nm.

III. RESULTS AND DISCUSSION

Figure 1 shows the normalized J_{ct} data of an YBCO+BSO sample on a $LaAlO_3$ substrate in an applied magnetic field of 0–12 T. Even though the J_{ct} at self-field was found to be around 1 MA/cm^2, the J_{ct} in the applied magnetic fields was found to be enhanced considerably. The increased J_{ct} in these films is believed to be due to the presence of 10 nm sized BSO nanoparticles that were formed in the YBCO films (to be discussed later).

It can be seen from Fig. 1 that the rate of fall in J_{ct} with the applied magnetic field in YBCO+BSO samples was very low as compared to regular YBCO samples. To illustrate this more clearly, alpha (α) measurements were taken using a vibrating sample magnetometer on YBCO+BSO and regular YBCO samples in the region where J_c is proportional to $B^{-\alpha}$, where B is the magnetic field. The temperature dependence of α over a temperature range of 20–77 K was measured and is presented in Fig. 2 for an YBCO control sample and two of the YBCO+BSO samples. It can be seen that the typical value for α for the YBCO control sample is 0.5 and is temperature independent. However, for the YBCO+BSO samples, α was found to be around 0.1 at low temperatures and it rises slowly to 0.3 at higher temperatures giving an average value of 0.2 in the temperature range of 20–77 K for YBCO+BSO samples. A low α value indicates that J_c drops with the magnetic field at a much lower rate. Such low values of α at 77 K were also reported in other pinned YBCO samples with $BaZrO_3$ (BZO) nanoparticles,[8] corroborating the data of low α value for these highly pinned YBCO+BSO samples.

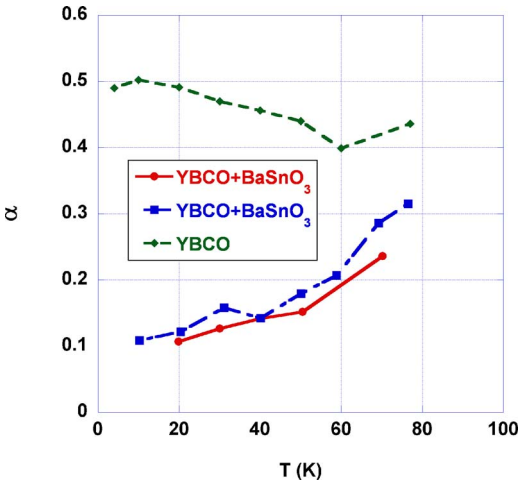

FIG. 2. Temperature dependence of α values for a control YBCO and YBCO+BSO samples on $LaAlO_3$ substrates.

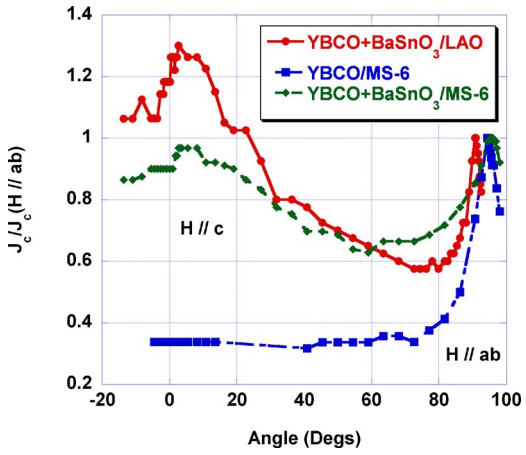

FIG. 4. Normalized J_{ct} with respect to J_{ct} in $H\|ab$ of YBCO+BSO samples as compared to regular YBCO at 77 K (LAO=$LaAlO_3$ substrate and MS-6=buffered metallic substrate).

Variations in J_{ct} with the applied magnetic field orientation to the sample normal at 77 K of an YBCO+BSO sample on a $LaAlO_3$ substrate are shown in Fig. 3. The angular dependence at various applied fields of 1, 3, and 5 T was compared. It can be seen that the J_{ct} in $H\|c$ orientation is higher than J_{ct} in $H\|ab$ orientation in all of these applied fields. The presence of peaks in the J_{ct} in $H\|c$ or H/ab orientation is commonly attributed to the presence of correlated defects.[6,7,14–16] Evidence of the *c*-axis correlated defects in YBCO+BSO is provided in more detail later during the TEM analyses.

To compare the relative increase in J_{ct} in $H\|c$ as compared to J_{ct} in $H\|ab$ in YBCO+BSO films, angular dependence data of normalized J_{ct} with respect to J_{ct} in $H\|ab$ are presented in Fig. 4. For comparison, data taken from a regular YBCO film on a buffered biaxially textured metallic Ni–W substrate (denoted as MS-6 in Fig. 4) are presented along with YBCO+BSO films on $LaAlO_3$ (denoted as LAO in the Fig. 4) and Ni–W substrates. It can be seen that the J_{ct} in $H\|c$ orientation is lower than J_{ct} in $H\|ab$ in regular YBCO samples. However, in YBCO+BSO samples, the J_{ct} in $H\|c$ is increased considerably. In this particular YBCO +BSO sample on $LaAlO_3$, the ratio of (J_{ct} in $H\|c$)/(J_{ct} in $H\|ab$) is about 1.3, whereas it is around 0.3 for regular YBCO.

Angular dependence of J_{ct} values of YBCO+BSO samples deposited on a buffered Ni–W metallic substrate was also measured to see if the improvements seen on $LaAlO_3$ can also be observed on the more practical buffered metallic substrates. Figure 5 shows the actual J_{ct} values measured at 77 K in an applied field of 1 T, whereas the normalized values with respect to J_{ct} in $H\|ab$ were shown earlier in Fig. 4. It can be seen that the J_{ct} in the $H\|c$ orientation is increased compared to the J_{ct} in the $H\|ab$ orientation similar to the behavior observed in the YBCO+BSO samples on $LaAlO_3$ substrates. This illustrates that the angular dependence with YBCO+BSO is independent of the substrate used and is directly caused by the nanoparticles and/or the defects created by them. It can be seen that the J_{ct} of YBCO+BSO samples processed on buffered metallic substrates (shown in Fig. 5) is slightly higher than the J_{ct} of YBCO+BSO samples processed on $LaAlO_3$ substrates (see J_{ct} at 1 T data in Fig. 3). The T_c of YBCO+BSO samples (90 K) processed on the buffered metallic substrates was noted to be slightly higher than the T_c of YBCO+BSO samples (88 K) pro-

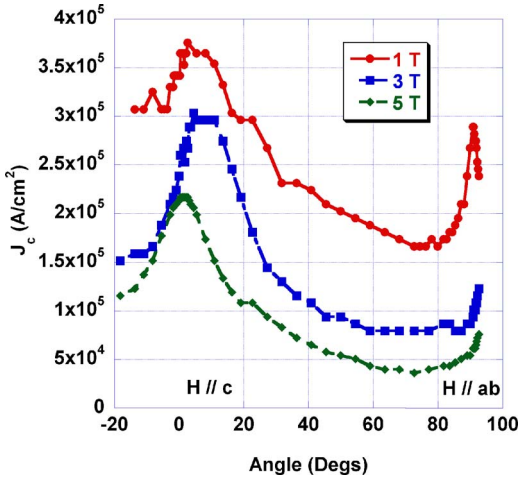

FIG. 3. Angular dependence of J_{ct} values of YBCO+BSO sample on a $LaAlO_3$ substrate at various applied fields of 1, 3, and 5 T at 77 K.

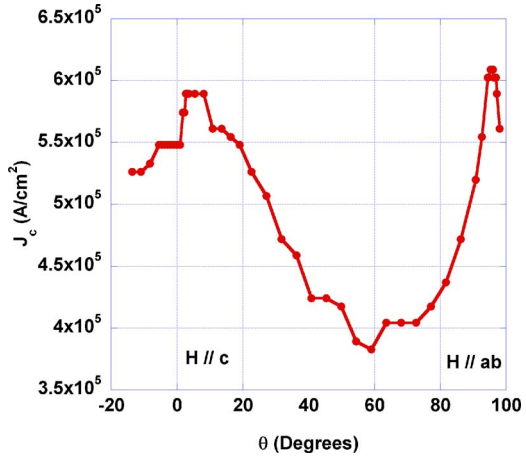

FIG. 5. Angular dependence of J_{ct} of an YBCO+BSO film on a buffered metallic Ni–W substrate in an applied magnetic field of 1 T at 77 K.

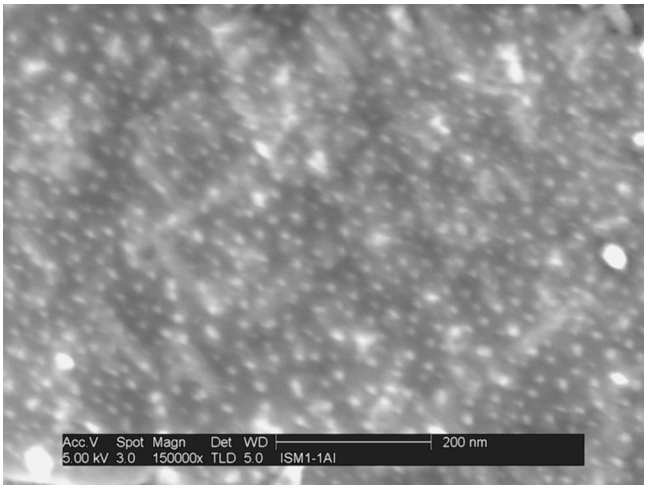

FIG. 6. Scanning electron micrograph of an YBCO+BSO sample on a buffered Ni–W metallic substrate.

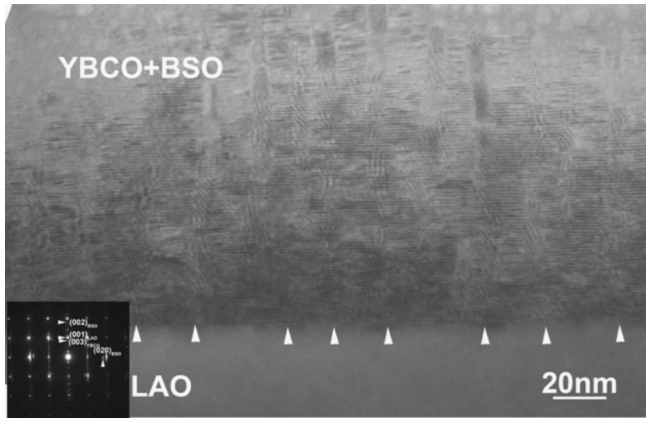

FIG. 7. Cross-sectional TEM image of an YBCO+BSO sample on a $LaAlO_3$ substrate. The particles were identified to be $BaSnO_3$ in the selected area diffraction pattern. Nanocolumns extending through the thickness, can be seen clearly, are marked by arrows.

cessed on $LaAlO_3$ substrates. The slight increase in J_c could probably be due to the T_c differences. However, the J_{ct} behavior in the applied magnetic field in YBCO+BSO films, such as the increase in the $H\|c$ orientation over $H\|ab$ orientation, is similar irrespective of the substrates used.

Microstructural characterizations were carried out to understand the observed J_{ct} angular dependence. Figure 6 shows a scanning electron micrograph of an YBCO+BSO film on a buffered metallic substrate. The micrograph shows the presence of high density of nanoparticles (~10 nm bright particles) in an YBCO+BSO sample. It is known that as the applied magnetic field is increased, the magnetic flux line density increases in YBCO, and so accordingly the number density of pinning centers required to interact with the magnetic flux lines also needs to be high for high field applications. The number density of pinning centers in the present sample was estimated to be $\sim 3.5 \times 10^{11}$ cm^{-2} from the SEM pictures, which corresponds to a matching field of ~7 T. This implies that at high magnetic field >5 T, the interaction between the flux lines and the particles was expected to be optimal.

In cross-sectional TEM images of the YBCO+BSO samples on $LaAlO_3$ substrates, high quality epitaxial growth of YBCO/BSO nanocomposites was observed. Figure 7 shows the cross-sectional bright field TEM image obtained from one of the samples. The presence of nanocolumns extending the entire thickness of the films can be clearly seen. The average spacing between the nanocolumns is around ~20–30 nm. In the literature, nanorod structures were observed in YBCO+BZO or YBCO+YSZ films made using PLD of premixed targets.[8,11] In this study, without using a premixed target but using only a dual sector target, similar microstructural features were obtained. Also noteworthy, the columns seem to be formed as continuous rods as opposed to a structure of self-assembled nanodots as indicated for other YBCO+BZO samples.[8] The corresponding selected area diffraction pattern (also shown as an insert in Fig. 7) clearly shows the high quality epitaxial growth of YBCO/BSO on LAO substrate. The diffraction dots from BSO can be clearly seen and indexed to be BSO (002) and (020), correspondingly (marked in Fig. 7). The epitaxial relations are determined to be YBCO(003)‖LAO(001)‖(BSO(002) and YBCO(020)‖LAO(020)‖BSO(020).

The fringe or moiré patterns in Fig. 7 around the rods are created due to the overlap of the YBCO and BSO lattices and their lattice mismatch. In order to reveal the detailed defect information at the interface of the YBCO/BSO, we conducted a detailed high resolution TEM (HRTEM) study on these cross-section samples. A high quality epitaxial growth of the YBCO/BSO nanocomposite was observed as shown in the HRTEM image given in Fig. 8. High density misfit dislocations and stacking faults generated at the interfaces of YBCO and BSO are shown in the corresponding fast Fourier transform (FFT) filtered image. The high density of these defects is strongly related to the high density of these BSO nanocolumns (spacing of ~20 nm), the large lattice mismatch between YBCO and BSO (~7%), and their vertical aligned orientation. From several cross-sectional images, the density of the misfit dislocations is estimated to be on the order of 1000 μm^{-2}. In the FFT image, it is clearly shown that the formation of the stacking faults is closely related to the generation of misfit dislocations. Therefore, the density of the stacking faults is on the same order of magnitude as that of the misfit dislocations. The presence of these high density columnar defects (nanocolumns) and the *c*-axis cor-

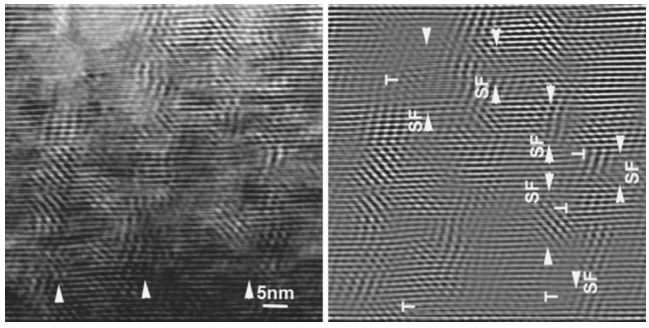

FIG. 8. High resolution TEM image of an YBCO+BSO film showing high density of defects. The FFT filtered image (shown on the right) shows the existence of high density of misfit dislocations and stacking faults at the YBCO/BSO interfaces.

related defects (misfit dislocations and stacking faults) could all contribute to enhance the J_{ct} in the $H \| c$ orientation.

IV. CONCLUSIONS

It is shown that high quality YBCO+BSO films can be formed using a dual sector PLD with a BSO sector method on both $LaAlO_3$ single crystal substrates as well as buffered Ni–W metallic substrates. These films were formed with high number density of nanoparticles (3.5×10^{11} cm^{-2}) and nanocolumns with high density of dislocations and stacking faults. These defects and nanoparticles improved the transport current density (J_{ct}) in both $H \| c$ and $H \| ab$ orientations.

ACKNOWLEDGMENTS

The Air Force Office of Scientific Research and the Propulsion Directorate of the Air Force Research Laboratory supported this work.

[1] P. N. Barnes, M. D. Sumption, and G. L. Rhoads, Cryogenics **45**, 670 (2005).
[2] T. J. Haugan, P. N. Barnes, R. Wheeler, F. Meisenkothen, and M. Sumption, Nature (London) **430**, 867 (2004).
[3] J. L. MacManus-Driscoll, S. R. Foltyn, Q. X. Jia, H. Wang, A. Serquis, L. Civale, B. Maiorov, M. E. Hawley, M. P. Maley, and D. E. Peterson, Nat. Mater. **3**, 439 (2004).
[4] C. Varanasi, P. N. Barnes, J. Burke, J. Carpenter, and T. J. Haugan, Appl. Phys. Lett. **87**, 262510 (2005).
[5] S. Kang, A. Goyal, J. Li, A. A. Gapud, P. M. Martin, L. Heatherly, J. R. Thomson, D. K. Christen, F. A. List, M. Paranthaman, and D. F. Lee, Science **311**, 1911 (2006).
[6] L. Civale, B. Maiorov, A. Serquis, J. O. Willis, J. Y. Coulter, H. Wang, Q. X. Jia, P. N. Arendt, J. L. MacManus-Driscoll, M. P. Maley, and S. R. Foltyn, Appl. Phys. Lett. **84**, 2121 (2004).
[7] B. Maiorov, J. L. MacManus-Driscoll, H. Wang, Q. X. Jia, P. Arendt, S. R. Foltyn, L. Civale, *Transactions of the ICMC*, edited by U. Balachandran [Adv. Cryog. Eng. 52, 73 (2006)].
[8] A. Goyal, S. Kang, K. J. Leonard, P. M. Martin, A. A. Gapud, M. Varela, M. Paranthaman, A. O. Ijaduola, E. D. Specht, J. R. Thomson, D. K. Christen, S. J. Pennycook, and F. A. List, Supercond. Sci. Technol. **18**, 1533 (2005).
[9] J. Hanisch, C. Cai, V. Stehr, R. Huhne, J. Lyubina, K. Nenkov, G. Fuchs, L. Schultz, and B. Holzapfel, Supercond. Sci. Technol. **19**, 534 (2006).
[10] C. Varanasi, R. Biggers, I. Maartense, D. Dempsey, T. L. Peterson, J. Solomon, J. McDaniel, G. Kozlowski, R. Nekkanti, and C. E. Oberly, Proceedings of the Materials Research Society Advances in Laser Ablation of Materials Symposium 1998, edited by R. K. Singh, D. Lowndes, D. B. Chrisey, E. Fogarassy, and J. Narayan, **526**, 263 (1998).
[11] P. Mele, K. Matsumato, T. Horide, A. Ichinose, M. Mukaida, Y. Yoshida, and S. Horii, Supercond. Sci. Technol. **20**, 244 (2007).
[12] T. A. Campbell, T. J. Haugan, I. Maartense, J. Murphy, L. Brunke, and P. Barnes, Physica C **423**, 1 (2005).
[13] C. V. Varanasi, P. N. Barnes, J. Burke, L. Brunke, I. Maartense, T. J. Haugan, E. A. Stinzianni, K. A. Dunn, and P. Haldar, Supercond. Sci. Technol. **19**, L37 (2006).
[14] L. Civale, B. Maiorov, A. Serquis, S. R. Foltyn, Q. X. Jia, P. N. Arendt, H. Wang, J. O. Willis, J. Y. Coulter, T. G. Holesinger, J. L. MacManus-Driscoll, M. W. Rupich, W. Zhang, and X. Li, Physica C **412–414**, 976 (2004).
[15] L. Civale, B. Maiorov, J. L. MacManus-Driscoll, H. Wang, T. G. Helesinger, S. R. Foltyn, A. Serquis, P. N. Arendt, IEEE Trans. Appl. Supercond. **15**, 2808 (2005).
[16] K. Develos-Begarinao, H. Yamasaki, M. Murugesan, Y. Mawatari, Y. Nakagawa, and J. C. Nie, Supercond. Sci. Technol. **18**, S266 (2005).